Carbohydrate Polymers 89 (2012) 1138–1149

Contents lists available at SciVerse ScienceDirect

Carbohydrate Polymers

journal homepage: www.elsevier.com/locate/carbpol

Effect of sectioning and water on resin-embedded sections of corn starch granules to analyze inner structure

Kazumi Tsukamoto, Toshio Ohtani, Shigeru Sugiyama*

Nanobiotechnology Laboratory, Food Engineering Division, National Food Research Institute, National Agriculture and Food Research Organization, 2-1-12 Kannondai, Tsukuba, Ibaraki 305-8642, Japan

ARTICLE INFO

Article history:
Received 11 February 2012
Received in revised form 27 March 2012
Accepted 28 March 2012
Available online 4 April 2012

Keywords:
Corn starch
Resin-embedded sections
Water effect
AFM
Inner structure

ABSTRACT

Resin-embedded sections and paired block surface of corn starch granules were observed using atomic force microscopy (AFM) and scanning electron microscopy to analyze the fine inner structure of starch granules and observe artifacts. Wrinkles were formed on the starch surfaces because of shear stress caused by the knife. Sectioned starches were isotropically expanded by water, and the growth rings and cracks between the growth rings were observed only on the sections. From this result, it was considered that the growth rings clearly showed shrinkage and/or corrosion of both edges of the ring during drying of the sections. Moreover, many small particles (width, ~30 nm; height, several nanometers) were clearly observed on the growth rings. These particles could be single clusters (~10 nm) of amylopectin molecules, considering the effect of the AFM tip radius.

1. Introduction

Starch is a biological resource produced mainly by green plants for energy storage and accumulates in the form of starch granules in tubers and seeds. Starch granules have various shapes with diameters ranging from submicrons to more than 100 μm depending on their source (Jane, Kasemsuwan, Leas, Zobel, & Robyt, 1994). Starch is a polysaccharide comprising numerous glucose units bound together by glycosidic bonds and consists of two main components—amylose and amylopectin. Normal plant starches, such as normal maize, rice, wheat, and potato, contain about 20–30% amylose and 70–80% amylopectin. The amylose-to-amylopectin ratio and the molecular and high-order structure of starch granules affect the physical and functional properties of the starch. Therefore, the inner structure of starch granules has attracted much attention.

Starch granules are not only an irregular disorganized aggregation of many polyglucose units but are also partially micro crystallite based on their X-ray diffraction (XRD) patterns. The crystal region mainly comprises ordered arrays of double helices formed by the side chains of amylopectin molecules (Gidley & Bociek, 1985; Imberty, Chanzy, & Pérez, 1988), and the crystal size is approximately 14.5 nm (Hizukuri & Nikuni, 1957). Furthermore, small angle X-ray (SAXS) and neutron scattering (SANS) have shown that a periodic structure of approximately 9–10 nm is present in various botanical starches (Blanshard, Bates, Muhr, Worcester, & Higgins, 1984; Blazek & Gilbert, 2010; Cameron & Donald, 1992; Jenkins & Donald, 1995; Jenkins, Cameron, & Donald, 1993; Oostergetel & van Bruggen, 1989; Sterling, 1962). The cluster model of the amylopectin molecule is widely accepted because a distribution of branch chain length of amylopectin is bimodal, which is different from the single modal distribution of glycogen (Hizukuri, 1986). The length of a cluster is approximately 27–28 glucosyl units, which is approximately 9.7 nm (Hizukuri, 1986) and in agreement with results from diffraction pattern and transmission electron microscopy (TEM) images (Gallant, Bouchet, & Baldwin, 1997; Putaux, Buléon, & Chanzy, 2000).

Starch granules have growth rings that are concentric ring structures similar to the annual growth rings of wood. Because of differences in corrosion caused by acid and enzyme treatments, it is considered that the growth rings consist of amorphous and semi-crystalline growth ring alternating lamellar structures (French, 1984; Jenkins & Donald, 1995; Martinl & Smith, 1995). Gallant et al. showed the existence of large (50–500 nm in diameter) and small (20–50 nm in diameter) particles called "blocklets" by scanning electron microscopy (SEM) of various botanical enzyme-treated starch granules (Gallant, Bouchet, Buléon, & Pérez, 1992) and suggested the blocklet model, which includes many clusters depending on blocklet size (Gallant et al., 1997). The blocklet model has recently been supported by SEM and atomic force microscopy (AFM) of the starch granule surface (Baldwin, Adler, Davies, & Melia, 1998; Krok, Szymońska, Tomasik, & Szymoński, 2000; Sujka

* Corresponding author. Tel.: +81 029 838 8054; fax: +81 029 838 7181.
E-mail address: ssugi@affrc.go.jp (S. Sugiyama).

0144-8617/$ – see front matter © 2012 Elsevier Ltd. All rights reserved.
http://dx.doi.org/10.1016/j.carbpol.2012.03.087

& Jamroz, 2009; Szymońska & Krok, 2003) and resin-embedded sections of starch (Baker, Miles, & Helbert, 2001; Neethirajan, Thomson, Jayas, & White, 2008; Parker, Kirby, & Morris, 2008; Ridout, Gunning, Parker, Wilson, & Morris, 2002; Ridout, Parker, Hedley, Bogracheva, & Morris, 2003, 2004, 2006). Ridout et al. (2003, 2004) reported that the starch structure in the blocklet model consists of amylopectin-based blocklets dispersed in an amylose-based supporting matrix because of the difference in swelling between crystalline and amorphous regions. Although the existence of blocklets is suggested by many studies of inner structure of starch granules, the blocklet has not been isolated until date (Pérez & Bertoft, 2010; Tang, Mitsunaga, & Kawamura, 2006).

Ultrathin sections have been observed by TEM to investigate the inner fine structure of biological materials such as cells and tissues. Currently, many AFM studies using resin-embedded sections of various biological samples have been conducted. In AFM no staining is required and there is no electron damage as observed in TEM; having advantages over other methods (Akhremitchev, Broun, Graner, & Walker, 2001; Amako, Takade, Umeda, & Yoshida, 1993; Chen et al., 2005; Graham et al., 2010; Li, Ji, Hu, & Sun, 2008; Matsko & Mueller, 2004; Matsko, 2007; Saoudi et al., 1994; Yamamoto & Tashiro, 1994; Zweyer, Troian, Spreafico, & Prato, 2008). Furthermore, AFM helps to obtained information regarding not only the surface but also section thickness. The effect of a knife when cutting sections has been observed in AFM images and not in TEM images (Amako et al., 1993). Therefore, AFM measurements of sections are performed with particular attention to artificial architecture. Li et al. (2008) reported that the best AFM imaging resolution is acquired by observing upper side sections, which are 50–100 nm in thickness. However, very few structural analysis studies of tissues, cells, and starch granules have considered the artifacts generated due to sectioning.

In this study, we observed resin-embedded sections and paired block surface of corn starch granules using AFM and SEM to analyze artifacts in the sections and observe the fine inner structure of starch granules. Wrinkles were formed on the starch granule surface because of shear stress caused by the knife. The sectioned starch granules were isotropically expanded to observe the growth rings, which became visible due to the effects of water. Moreover, embedding resin and starch granules were sectioned with elastic deformation. Analysis of the inner structure of the starch granules was performed considering the above-mentioned artifacts, knife marks, and chattering. As a result, many small particles (~30 nm), which could be a single cluster of amylopectin molecules, were clearly observed on the growth rings.

2. Experimental

2.1. Materials

Normal corn starch (cat. no. S-4126) having an amylose content of approximately 27% (product information) was purchased from Sigma–Aldrich, Inc. (St. Louis, MO, USA). The corn starch was used without purification or specific treatment. Technovit 7100 and 3040 resins (Heraeus Kulzer, Wehrheim, Germany) were used for embedding and for hardening, respectively.

2.2. Resin-embedding of starch granules

Starch was not fixed with glutaraldehyde or paraformaldehyde. First, the starch was dehydrated through an ethanol series (30%, 50%, 70%, and 99.5%) for 20 min each. Infiltration was performed with a resin diluted stepwise with ethanol (20% resin for 30 min, 50% resin for 30 min, and 80% resin for 30 min). Subsequently infiltrated starch was dipped in Technovit 7100 solution A (mixture of Technovit 7100 and harder I) overnight. All treatments were performed on a rotator at room temperature. After solution A was replaced with a mixture of solution A and harder II, the mixture, which included starch, was poured into a plastic capsule. Polymerization of the resin was performed on water with a floater to lower the cure temperature. Finally, the unhardened region around the surface of the resin block was cured completely with Technovit 3040 after the resin had almost hardened.

2.3. Sectioning

Thin sections (~1 μm) were obtained using an ultramicrotome (Ultracut E, Reichert-Jung, Wien, Austria) equipped with a diamond knife (hist, Diatome, Biel, Switzerland) at a speed of 1 mm/s. Immediately after sectioning, the sections were transferred to a Petri dish containing MilliQ water with a sharpened bamboo skewer. The sections were collected on a glass slide using a platinum loop after they were kept on water for more than 30 min to create a sufficient water effect, and then the slide was dried on a heat block at 40 °C. The section has two surfaces: a lower surface in contact with water and an upper surface in contact with air. The upper surface on water was consistently observed by AFM. The sectioned surface of the resin block was trimmed into an asymmetric trapezoidal shape to distinguish the A surface from the B surface (Fig. 1). Sectioning was performed from the bottom of the trapezoid to the top.

2.4. Atomic force microscopy

An AFM (NanoWizard II, JPK instruments, Berlin, Germany) instrument mounted on an inverted optical microscope (TE2000-U, Nikon, Tokyo, Japan) was used to image the section and block surface (A surface). AFM imaging was performed using the intermittent contact mode in atmospheric air with stiff silicon cantilevers (OMCL-AC160TS, Olympus, Tokyo, Japan), which had a nominal spring constant of approximately 42 N/m and a nominal frequency of approximately 300 kHz. The sectioning direction and face (A or B surface) of the sections were confirmed by phase-contrast microscopy and from the shape of the sections and the knife marks observed on AFM images.

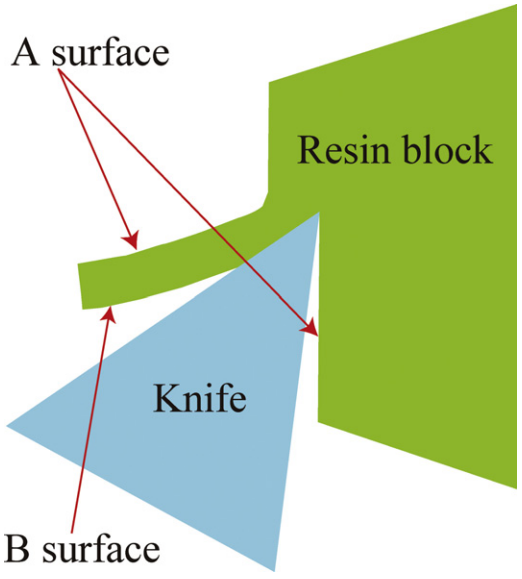

Fig. 1. Scheme of sectioning a resin block using an ultramicrotome (a side view). The section has two faces: the A surface (upper side) and the B surface (lower side). The block has only the A surface.

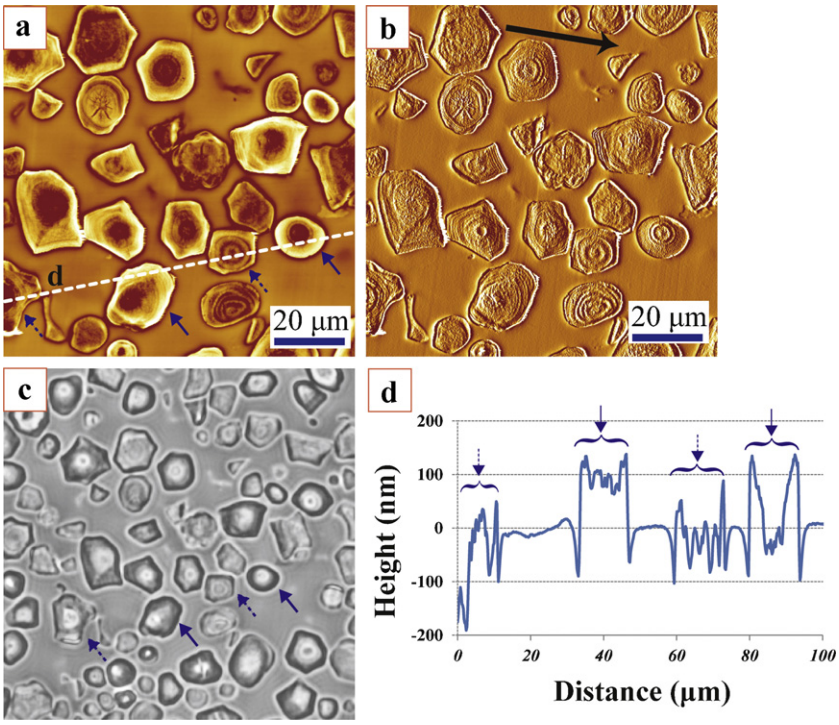

Fig. 2. AFM and optical phase-contrast image of a resin-embedded section (0.5 μm in thickness, A surface) of corn starch and a cross section of AFM height image. (a) and (b) is a height image and error signal image at the same region. The solid arrow indicates the sectioning direction in (b). (c) Optical microscopic image (phase contrast) of the section at the same region in (a). (d) Cross section along the dashed line in (a). Solid and dashed arrows indicate the same starch granules in (a), (c), and (d). Scale bars as indicated.

2.5. Scanning electron microscopy

SEMs (JSM-5600LV and JSM-7600F, JEOL, Tokyo, Japan) were used to image the corn starch granules, the section and the sectioned block surface. To avoid sample damage induced by accelerated electron beam and degradation of SEM images by accumulation of electrons, all samples were coated with gold (JFC-1500, JEOL) or osmium (OPC60A, Filgen, Nagoya, Japan), and all SEM measurements were performed below 5 kV. When the same sample and the same position of the section and block surface were observed by AFM and SEM, AFM measurements were inevitably performed before SEM imaging.

3. Results and discussion

3.1. Evaluation of the section

Various artifacts caused by sectioning of starch granules were evaluated. Fig. 2a–c show the topographic and error signal images of 0.5-μm section of corn starch granules and a phase-contrast images at the same position. Both AFM images clearly indicate the shape of the granules and growth rings. The shapes observed were typical of corn starch, approximately 15 μm in size. The edges of the sectioned granules were approximately 150 nm higher than the resin surface (Fig. 2d). In contrast, the starch surface at the hilum near the center of the granules was lower than the resin surface. There were two types of sectioned granules: dark granules, which had strong contrast, and tinted granules, which had low contrast (Fig. 2c). In comparison to the AFM height image, the dark and tinted granules meant a difference in height from the resin surface: higher (∼150 nm) and lower (∼100 nm), respectively.

The edges of different sections were observed to measure accurate section thickness (Fig. 3). The resin was thinner than the ultramicrotome setup value (0.5 μm): approximately 300 nm (Fig. 3c). The top of the starch surface was approximately 420 nm, which was near the setup value. Thus, the starch surface may have become higher than the resin surface due to resin shrinkage. Fig. 3d shows the magnified error signal image of a granule as indicated in Fig. 3b. The island at the center of the granule had a weak knife mark (Fig. 3d). Although strong knife marks were clearly observed on starch granules and resin (data not shown), weak knife marks were observed only on the resin surface due to relief on the cross-section surface of the granules such as the growth rings and other fine structures (Fig. 3d), indicating that the resin surface was smoother than the surface of the sectioned granules. Therefore, the island included the resin that had infiltrated the granule cavity. Infiltration of the resin into some granules was observed (Fig. 3a and b; indicated by black arrows).

There were many wrinkles in a direction perpendicular to the knife marks on the sectioned surface of almost all granules, but not on the resin surface without reference to the A or B surface as shown in Fig. 3d. These scattered wrinkles were seen only on a part of the cross-section area of the granules (Fig. 4) and were not seen on the block surface. Thus, these wrinkles were not considered artifacts of chattering, but rather cracks formed by stress from the knife when the section was bent over and deformed by the knife.

To evaluate deformation in starch granules from the section, we observed two serial sections (A and B surfaces) by AFM (Fig. 5a and b). For easy comparison, the AFM image of the B surface was reflected and rotated (Fig. 5b). On both surfaces, parts of the granules were higher than the resin area at the same height as the images in Fig. 2, and no difference was observed in roughness from the height histograms (data not shown). Some granules had a central depression in both the A and B surfaces. Therefore, the A surface did not coincide three-dimensionally with the B surface. Thus, the granule contour was extracted and compared with regard to A and B surfaces to analyze two-dimensional compression or deformation of granules (Fig. 5c and d). Each outline was placed on the same

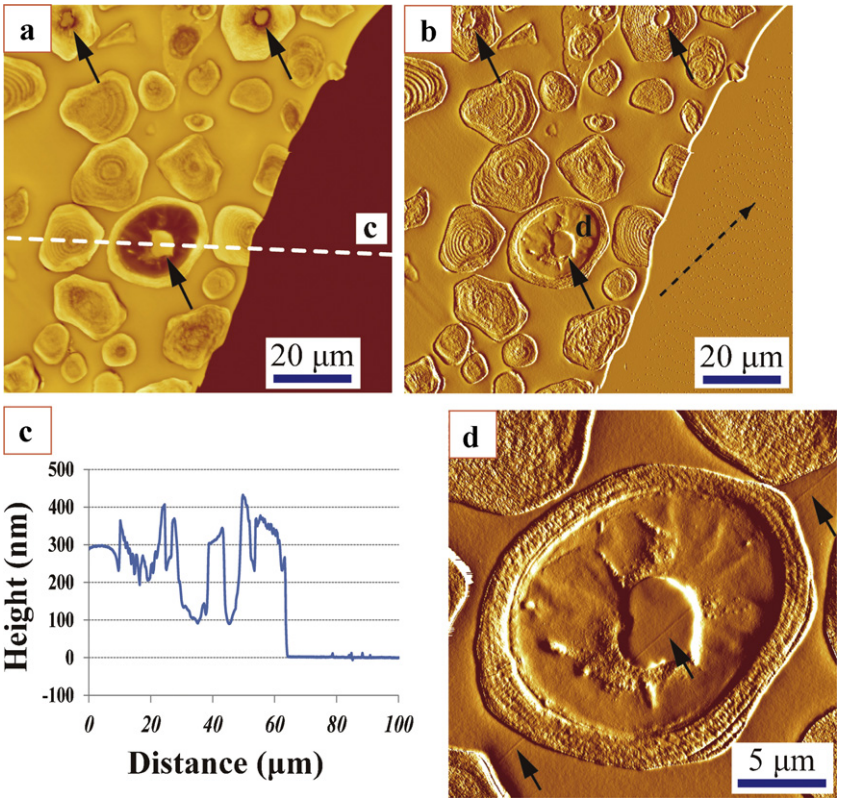

Fig. 3. AFM height and error signal images of the resin-embedded section (0.5 μm in thickness, A surface) of corn starch and a cross section at the edge of the section. (a and b) Height and error signal images at the same region. Black arrows indicate that the resin infiltrated the cavity of starch granules at the hilum in (a) and (b). The dashed arrow shows the direction of sectioning in (b). (c) Cross section along the dashed line in (a). (d) Enlarged error signal images of the granules is imaged. Three black arrows indicate the knife marks. Scale bars as indicated.

plane with the relative position fixed so that the overlapping area of both surface outlines was maximized with a central focus on the granule indicated by the solid arrow (Fig. 5c). As shown in Fig. 5c, partial displacement of granules was clearly observed. However, the A surface outlines almost coincided with the B surface outlines, after unfixing the relative position on the B surface, and each outline of the B surface was transferred to the A surface outline to maximize overlap (Fig. 5d). Consequently, not much difference in the size and shape of granules was observed between the A and B surfaces.

Fig. 5e is a scatter plot of the relationship between the area of the sectioned granules and the ratio of the area on the A surface to that on the B surface. No change was seen in the distribution even if the section thickness was changed. The distribution ratio was less than ±10% in almost all granules. As the granule size decreased, the ratio varied widely, indicating that there would be great variability among small size granules. Thus, it was considered that compression and deformation may not have been due to sectioning.

Both the block surface (A surface) and the section (B surface) paired with the block surface were observed by SEM to investigate the effect of water on the section (Fig. 6). Fig. 6a2 and b2 are SEM images of the block surface after the sections in Fig. 6a1 and b1 were sectioned at 0.5 and 0.9 μm, respectively. As shown in Fig. 6a3 and b3, the sections were somewhat larger than the block surfaces. The magnification percentage of each section was 125% in area for the 0.5-μm section and 115% for the 0.9 μm section. Both sections were

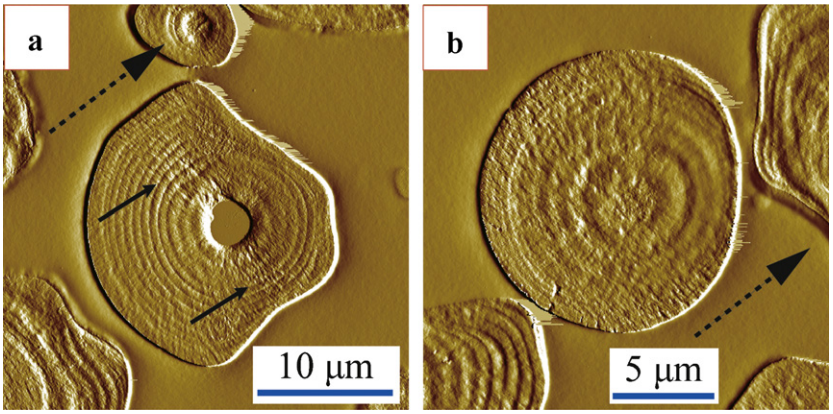

Fig. 4. AFM error signal images of the resin-embedded section (0.5 μm in thickness, A surface) of corn starch. Starch granules in (a) and (b) were from the same section. The dashed arrow shows the direction of sectioning in (a) and (b). Dispersed wrinkles indicated by the solid arrow were seen partially on the starch granules but not on the surface. Scale bars as indicated.

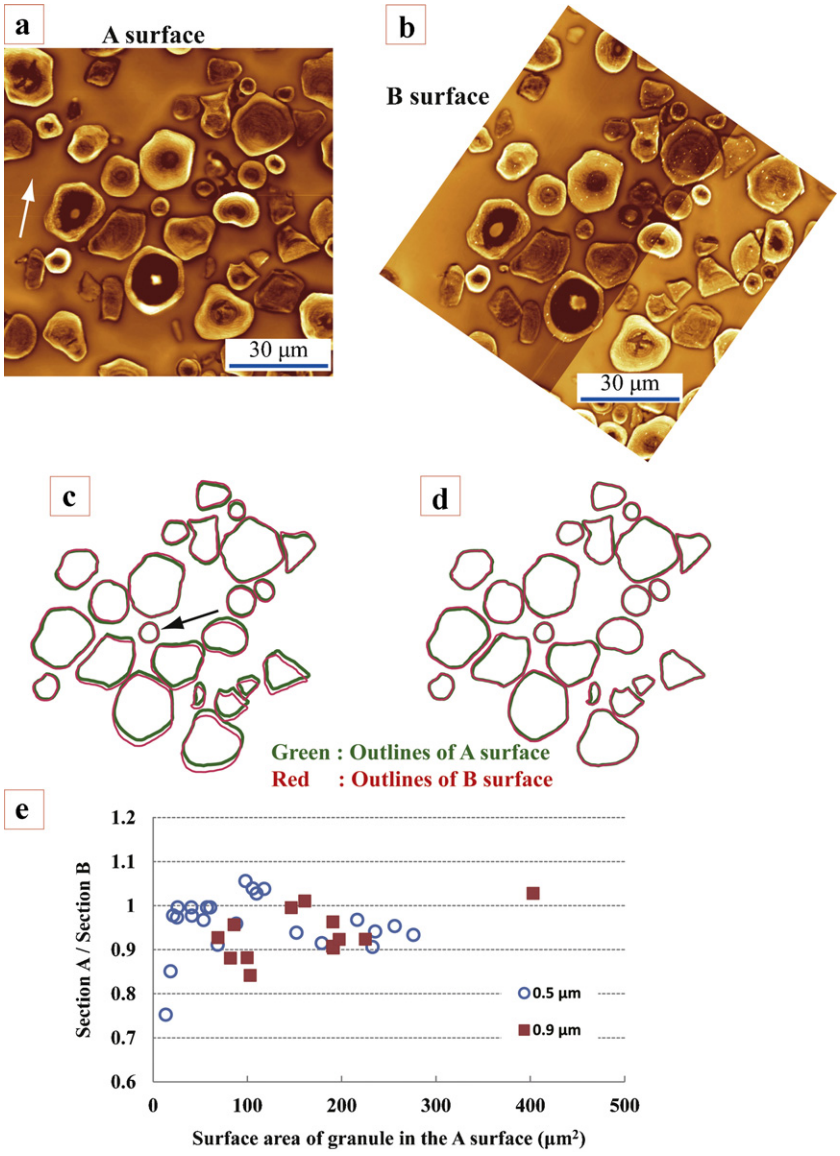

Fig. 5. Comparison of the A surface with the B surface of a section by AFM height images of continuous corn starch sections (0.5 μm in thickness). (a) AFM height image of the A surface. White arrow indicates the direction of sectioning. (b) AFM height image of the B surface paired with the A surface. This image was reflected and rotated to compare it with the A surface. (c) Maximum overlapping display of outlines of the sectioned starch granules of both AFM images fixed relative to the position of each surface. Solid arrow indicates the center of overlap. Green and red outlines indicate the outlines of the A and B surfaces, respectively. (d) Overlapping display of outlines of the sectioned starch granules of both AFM images after fixed relative position of outlines of the B surface were unlocked and each outline was moved to maximize overlapping of outlines in the A surface. (e) Scattering diagram of the area ratio by the area of each starch granule. Open blue circle and filled red square indicate the data obtained from 0.5 and 0.9 μm sections, respectively. Scale bars as indicated.

nearly isotropically expanded, and the thin section was much wider than the thick section. This stretch in the section may have been because of the surface tension of water. This phenomenon induces considerable movement of the granules. As a consequence, a difference in granule position was observed between the A and B surfaces as shown in Fig. 5c. The displacement of the granules was inhomogeneous according to resin hardness and density of granules in the section.

There was a slight difference in expansion of the section because of thickness. Previous studies have reported that the topographical contrast on an AFM image of a section surface is altered by the knife (Amako et al., 1993), the hardness of the embedding resin (Matsko & Mueller, 2004), the section thickness, and the section surfaces (Li et al., 2008). In particular, Li et al. (2008) reported that the upper side (A surface) section of epoxy resin-embedded 50–100 nm thick cells was suitable for AFM imaging. In contrast, the normal minimum thickness of Technovit 7100 resin is approximately 300 nm (ultramicrotome setup value); hence, the Technovit 7100 resin was much softer than the epoxy resin previously used. Thus, we attempted AFM observations using three thicknesses of the upper side (A surface) of the section from 0.3 μm (Fig. 7). As sectioning thickness decreased, the domains of granules that were lower than the resin increased, and the growth rings became visible (Fig. 7a1, a2, b1, b2, c1 and c2). Artifacts that were caused by folding of the thin section (Baker et al., 2001; Gallant & Guilbot, 1971; Mussulman & Wagoner, 1968) were seen in the 0.3 μm section, as indicated by the solid arrows (Fig. 7a1 and a2). In contrast, almost nothing was seen in the 0.5- and 0.9-μm sections. Some starch cavities and resin infiltration occurred in the center cavities of granules (Fig. 7a2, b2 and c2). Whistler, Goatley, and Spencer (1959) reported two shapes of corn starch granule cavities. In our study, the circular and irregular type cavities were observed.

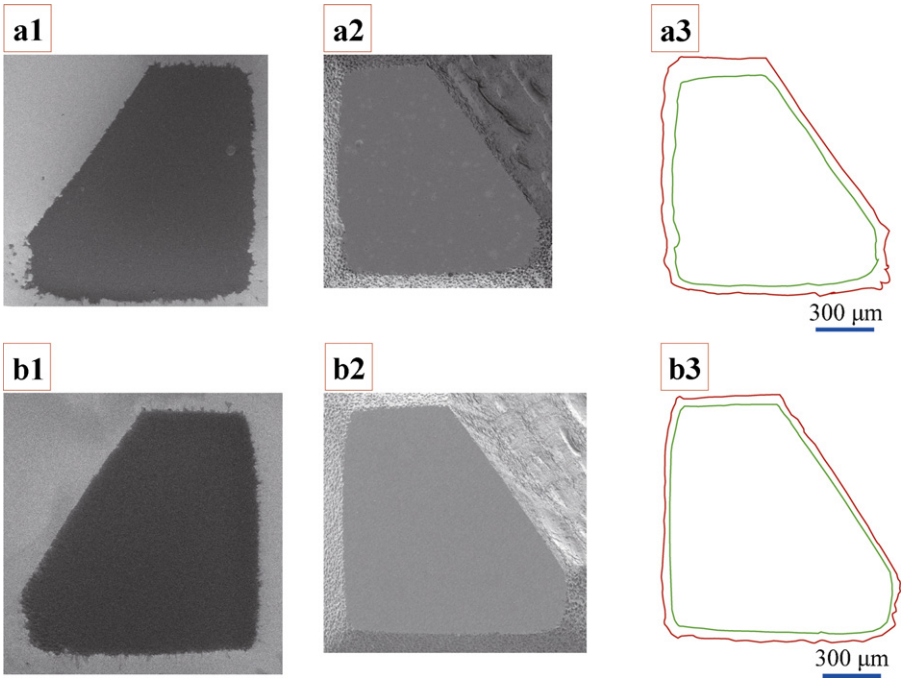

Fig. 6. Comparison of the complete section with the complete block surface by SEM images of corn starch section. (a1) SEM image of the 0.5 μm section. (a2) SEM image of the block surface after the section in (a1) was cut. (a3) Overlap of both outlines of the block and section in (a1) and (a2). Red and green outlines are the outline for the section and block, respectively. (b1) SEM image of the 0.9 μm section. (b2) SEM image of the block surface after the section in (b1) was cut. (b3) Overlap of both outlines of the block and the section in (b1) and (b2). Red and green outlines are the outline for the section and block, respectively. Scale bars as indicated.

The actual thicknesses of 0.3-, 0.5-, and 0.9-μm sections were 171 nm, 314 nm, and 515 nm in the resin area, respectively, from the cross sections shown in Fig. 7a1, b1 and c1 (Fig. 7a3, b3 and c3). Moreover, height of protrusion from the resin surface in the starch region was approximately 50, 150, and 200 nm. The sums of the resin height and starch protrusion, which were approximately 220 nm (for the 0.3-μm section), 460 nm (for the 0.5-μm section), and 720 nm (for the 0.9-μm section), were close to the setup thickness. Although there was variation in the height of the starch protrusion, the resin thickness of the 0.5-μm sections was equivalent with the resin thickness in Fig. 3. Hence, the average thickness at the resin region was calculated with each setup thickness (Fig. 8). The resin thickness increased approximately linearly as the ultramicrotome setup value increased, whereas the shrinkage ratio (resin thickness/setup thickness) appeared to remain constant.

3.2. Comparison of starch granule size and shape between the block surface and the section

AFM and SEM measurements of the block surface (A surface) were performed to examine the effect of water on starch granules after preparing the 0.5-μm section (Fig. 9). No starch granule growth rings were observed without water treatment as described in a previous report (Ridout et al., 2004) (Fig. 9a and b). Depressions were present at the center of starch granules, except for the granule marked by the circle at the upper right corner (Fig. 9a). The error signal image shows that the smoothness of the sectioned surface of the granule in the upper right corner was different between the center and periphery. The difference was seen as a different contrast on the SEM image (Fig. 9d). The smooth area at the center of the granule was the resin surface. Therefore, a depression was not observed in this granule. The depth of the depression was approximately a few hundred nanometers for both the block surface and the 0.5-μm section surface (star marks in Figs. 7b3 and 9c). It was considered that water hardly affected depressions of granules when the section was floated on water. Additionally, a few sectioned granules had a depression depth with ca. 500 nm (triangle and square marks in Fig. 9c). These depressions showed clear cavities in SEM images. The real depth of the depressions was significantly deeper than the value measured by AFM, because the AFM tip may not have touched the bottom of all depressions. It was determined from SEM images of the block surface that all cavities were not filled with the resin.

SEM images of a pair of interfaces of the section (B surface) and block surface (A surface) were performed for fine analyses of water effects with respect to shape of starch granules (Fig. 10). By comparing SEM images of the block and section at the same area, resin-infiltrated granules (surrounded by a dashed circle 1, 1′) and granules without infiltrated resin (surrounded by a dashed circle 2, 2′) into the irregular type cavity were clearly identified (Fig. 10a1 and a2). Two granules surrounded by a dashed circle 3, 4, which had many small pores or defects at the core, were observed brightly (Fig. 10b1). Generally, secondary electrons are likely to be emitted at the edge and area where gaps, cavities, and pores exist. Actually, parts of pits or pores were observed as white and bright. The pitted area of granules in the section decreased after sectioning and spreading on slide glass (Fig. 10b2 and AFM height image; data not shown). Nikuni and Whistler (1957) indicated that many pores may originate from the attack of plant enzymes. Gelatinized starch is digestible by enzyme. Therefore, the disruption of pitted area by water may be the melting and/or gelatinization when the section was spread on water. These small pores existed not only at the center of granules but also at the periphery (Fig. 10b1). The pores were a few hundred nanometers in diameter and very close to the surface pore size (Fannon, Hauber, & BeMiller, 1992; Sujka & Jamroz, 2010). The pores were very similar to the cross section of the channel in starch granules observed by Huber and BeMiller (1997), Jenkins and Donald (1995). Although many pores were seen in our SEM images, recognizable channels were not observed on our block surfaces. If

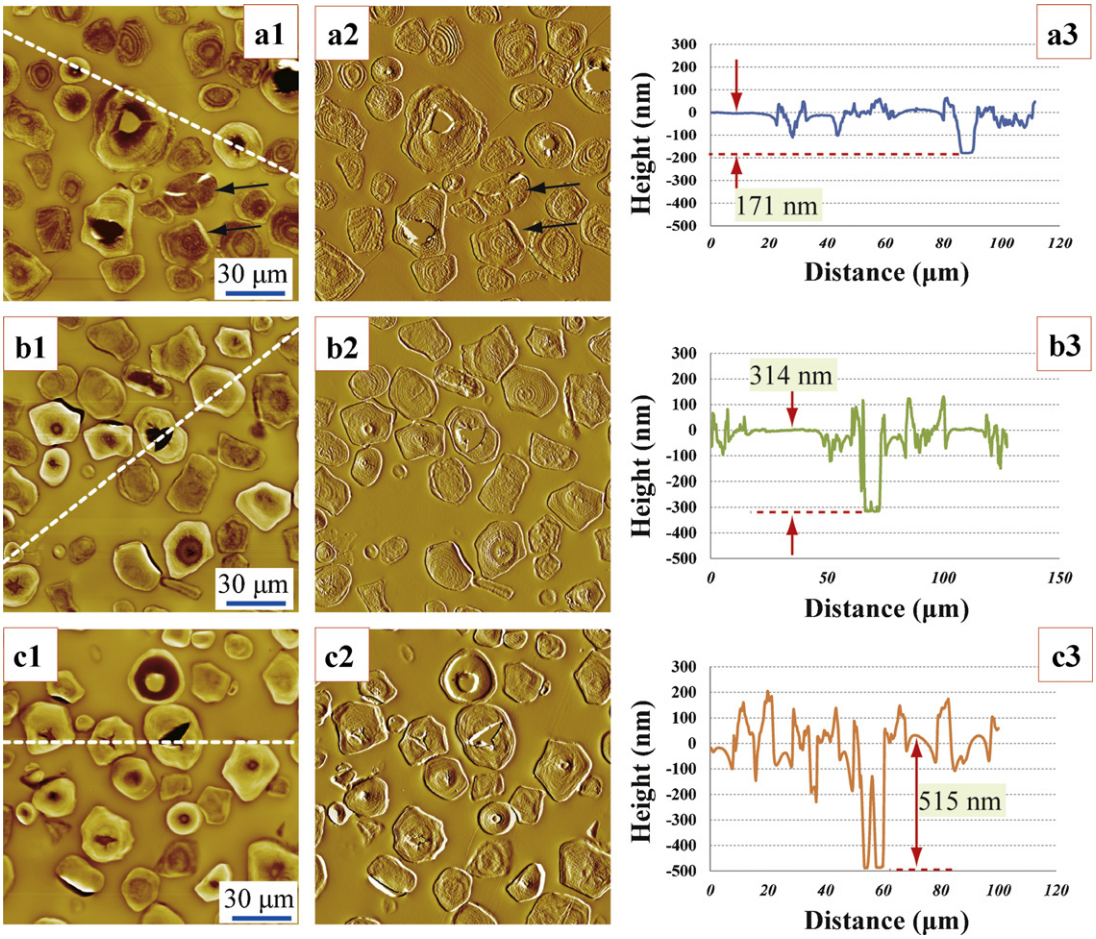

Fig. 7. AFM height and error signal images of the resin-embedded section of starch and cross section. The three sections were cut to different thicknesses. (a1, a2) AFM height and error signal image of the 0.3 μm section. Some folding artifacts were observed in a few starch granules in only the thinnest section indicated by the solid arrow at the edge and inside of granule. (a3) Cross section along with the dashed line in (a1). (b1, b2) AFM height and error signal image of the 0.5 μm section. (b3) Cross section along with dashed line in (b1). (c1, c2) AFM height and error signal image of the 0.9 μm section. (c3) Cross section along with dashed line in (c1). Scale bars as indicated.

the pore was a result of digestion, the connection to a continuous hole may become a channel. The existence of channels may depend on the degree of starch granule digestion. Neither the channels nor the pores were observed in the section of starch granules because of the effect of water.

Starch granules in the section became larger compared to those on the block surface. In particular, granules with a defect, cracked cavity, and a pored structure appeared to grow wider. Hence, measuring the shape and size of starch granules between the block surface (A surface) and section (B surface) was performed as the thickness of the section was changed (Fig. 11a–c). Fig. 11a–c shows the SEM images of the section overlaid on the outlines of the granules for the block surface (black dashed line) and for the section (red line). The magnitude of the change decreased as the thickness of the section increased. The direction of expansion in the granules did not depend on the sectioning direction; almost all granules showed isotropic expansion. However, some granules were anisotropically elongated in the long axis direction due to defects in the inner starch structure, cavity, and pore. Both the resin and starch granules sectioned had isotropically expanded compared with one of the block surfaces when the section was wetted. In our study, obvious compression was not observed based on the sectioning direction. Even if there was compression, it was expected that the deformation amount was very small.

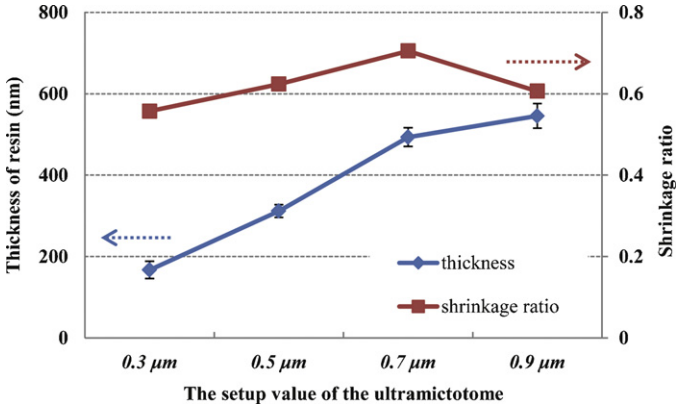

Fig. 8. The average of section thickness at the resin region and the shrink rate of the resin by the setup thickness.

To consider the difference in the expansion rate by the area of the starch granules, the cross section area of starch granules, both the block and the section surface, was measured in every thickness of the section (Fig. 11d). Averages of the expansion rate were 1.71 ± 0.16 for the 0.3 μm section, 1.34 ± 0.13 for the 0.5-μm section, and 1.30 ± 0.18 for the 0.9-μm section, respectively. From these data and Fig. 11d, it can be concluded that the expansion rate decreased as the thickness of the section increased. The expansion rate was relatively constant over 100 μm^2 in area of granules

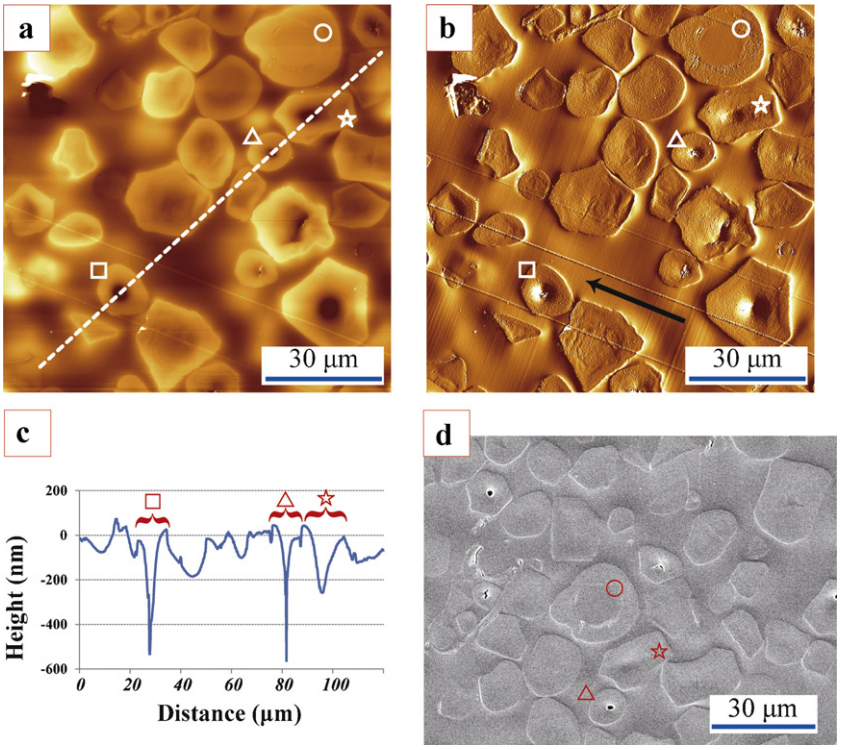

Fig. 9. AFM and SEM images of the resin-embedded block surface of starch granules and a cross section of the AFM height image after the 0.5 μm section was cut. The block sample was coated with osmium using an SEM osmium plasma coater. (a and b) AFM height and error signal images of the block surface. Solid arrow indicates direction of sectioning in (b). (c) Cross section along with the dashed line in (a). (d) SEM image of the block surface after AFM measurements. The specific mark indicates the same granules in each figure and the cross section.

with or without defects. This indicated that the expansion of granules may be restricted by expansion and contraction of the resin. Because the coefficient of expansion depends on the thickness of the section, it is considered that the expansion of both the resin section and the starch granules due to water decreased in the thicker section.

4. Sectioning model

It is necessary to consider artifacts of sectioning when the interface fine structure is evaluated in the section. In particular, it is very important to determine how the section is cut from the resin block by the diamond knife including the starch granules. Until

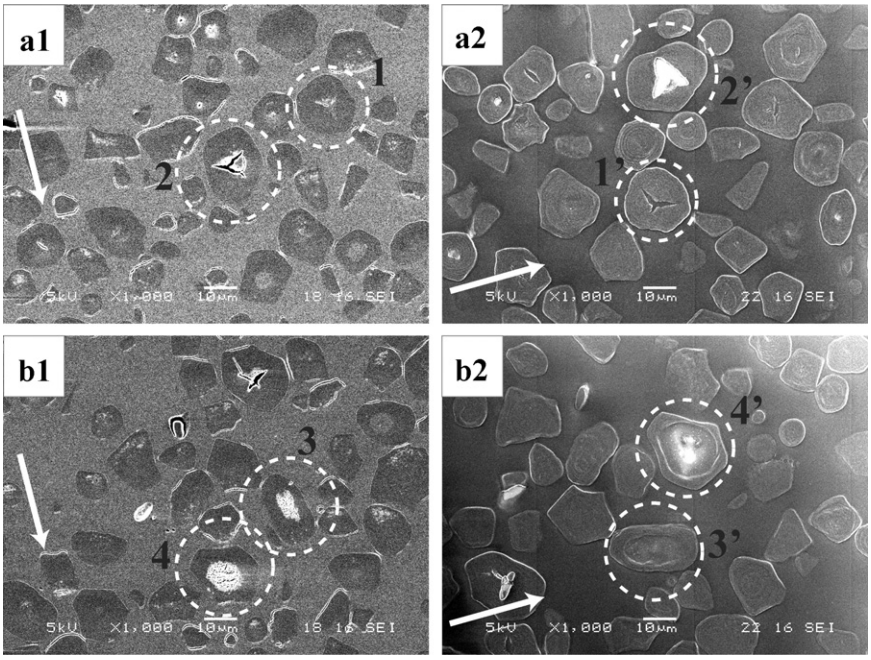

Fig. 10. Comparison of SEM images between the block surface and section of corn starch (0.9 μm in thickness). (a1 and a2) A pair of the block surface and section. (b1 and b2) A pair of the block surface and section. White arrows indicate direction of sectioning in all SEM images. Starch granules surrounded by dashed circles, 1, 2, 3, and 4 in block surface pairs with starch granules surrounded by dashed circles, 1′, 2′, 3′, and 4′ in section surface. Scale bars as indicated.

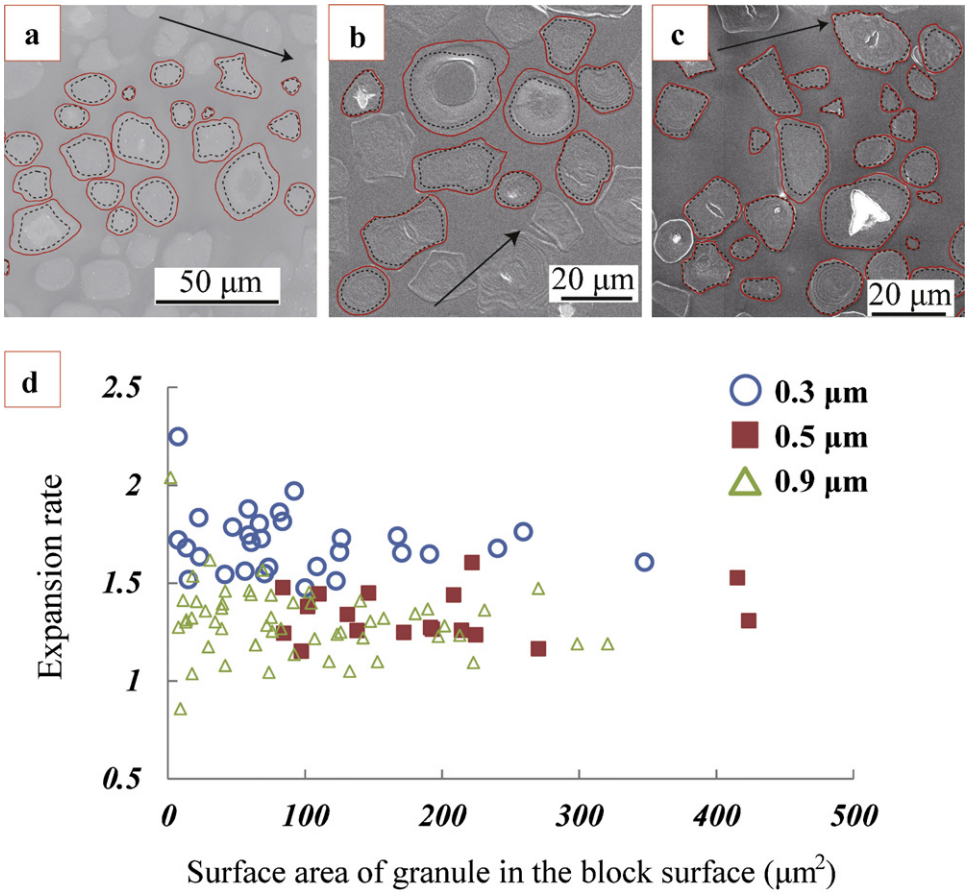

Fig. 11. SEM images of the section of corn starch granules based on section thickness and a scattering diagram of the expansion rate of starch granules by water. SEM images were overlapped by outlines of starch granules of both block surface and section. Red and dashed black outlines are the section and block surface outlines, respectively. (a) 0.3 μm section. (b) 0.5 μm section. (c) 0.9 μm section. Black arrows indicate the sectioning directions in (a–c). (d) Scattering diagram of expansion rate. Open blue circle, filled red square and open green triangle indicate the data obtained from 0.3, 0.5 and 0.9 μm sections, respectively.

now, two sectioning models have been proposed to obtain better section (Acetarin, Carlemalm, Kellenberger, & Villiger, 1987). One is the cleavage model in which a microscopic crack forms at the top of the knife edge in a relatively harder resin. The other is true sectioning model with softer resin such as metal cutting. Normally, sectioning begins with contact of the knife, and elastic and plastic deformation of the resin block by shear stress follows. Finally, a part of the section is formed when the block cannot resist the shear stress (Fig. 12a). The elastic and plastic deformation is small and cleavage arises from the knife edge when a harder resin is used. In our experiments, the embedding resin shrunk to about 60% of the entire thickness. The average expansion rates on the 0.5-μm section were approximately 1.34 for starch granules and approximately 1.25 for the section, respectively. If the expansion rate of the entire section including the granules is 1.3 and the volume of the section is not changed by expansion, the thickness of the section will be 0.385 μm. However, the actual average thickness of the section was slightly smaller at about 0.312 μm in the resin area as compared to the value of the theoretical calculation, which was 0.385 μm. This indicated that resin shrinkage was influenced

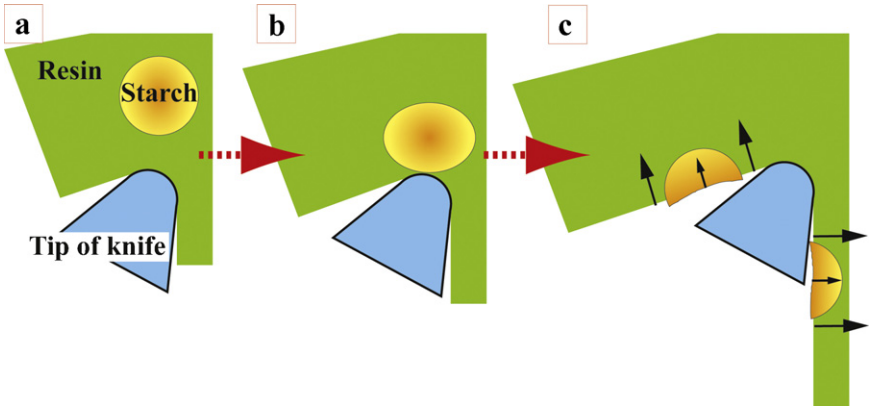

Fig. 12. Scheme of sectioning with elastic deformation from a side view. In real scale, the starch granule and curvature radius size were approximately 15 μm and 10 nm, respectively. The starch granule was drawn much smaller for ease of understanding. Solid arrows indicate the direction of shrinkage after sectioning.

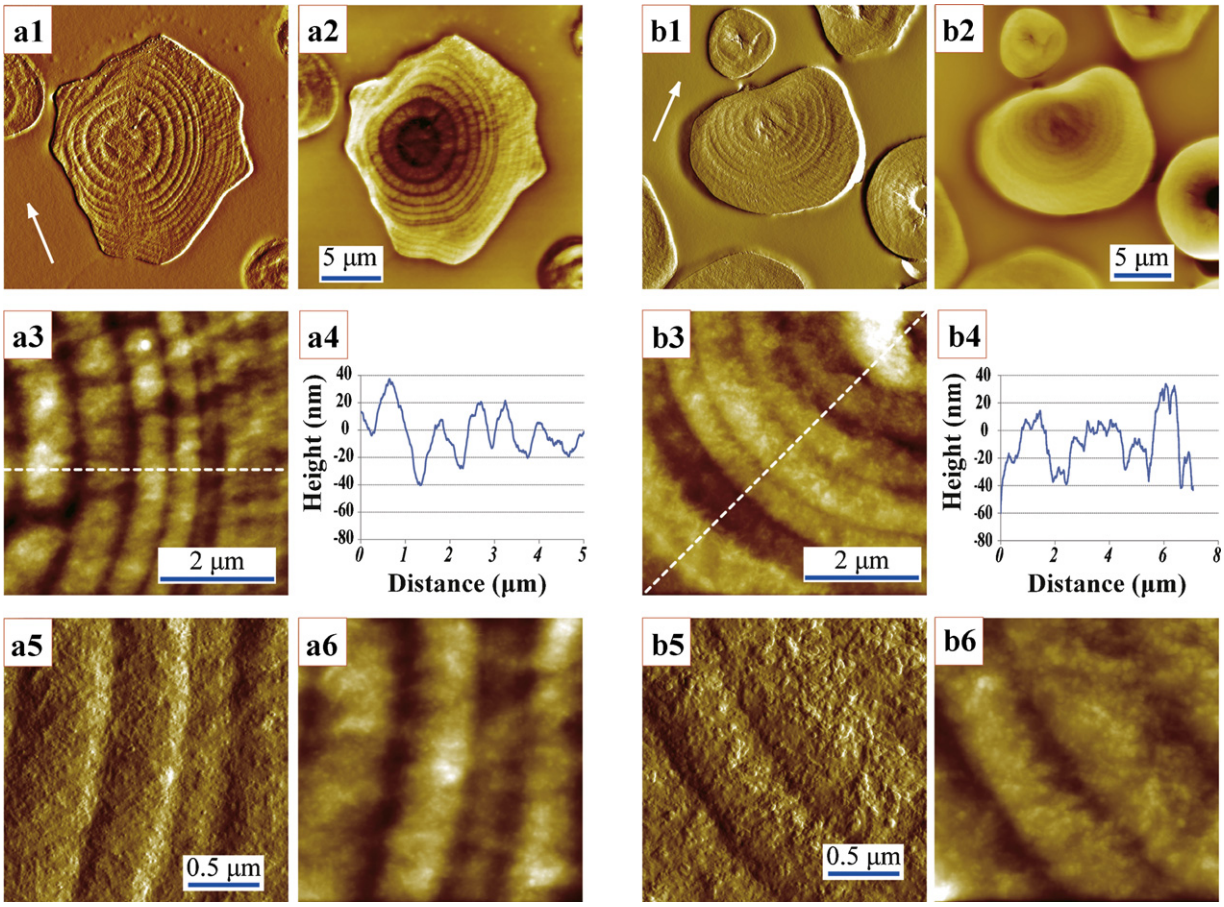

Fig. 13. AFM error signal and height images of a resin-embedded section [0.3 μm (a1–a6) and 0.9 μm (b1–b6) in thickness, both section's surface is A surface] of starch and the cross section. (a1 and a2) AFM error signal and height images of the complete granule. White arrow indicates the sectioning direction. (a3) AFM height image magnified at the center of (a2). (a4) Cross section along the dashed line in (a3). (a5 and a6) AFM error signal and height image magnified at the center of (a3). (b1 and b2) AFM error signal and height images of the complete granule. White arrow indicates the sectioning direction. (b3) AFM height image magnified at the center of (b2). (b4) Cross section along the dashed line in (b3). (b5 and b6) AFM error signal and height image magnified at the center of (b3). Scale bars as indicated.

not only by expansion of the section but also by other factors. A main factor would be the sectioning with maintenance of the elastic deformation of resin. Consequently, the resin is cut and shrinks after elongation of the resin by the pressure of the knife edge. Based on the morphology of the block surface, it was considered that water had little influence on resin shrinkage. Additionally, starch granules will have this elastic deformation and be sectioned with elastic deformation (Fig. 12b). The center of granules will shrink similar to the resin after sectioning in the absence of the effect of water (Fig. 12c). From the above speculation and comparison of both the starch (~15 μm) and the knife edge (~2 nm) (Black, 1971) in sizes, our model supported the true sectioning model. It was considered that resin shrinkage would occur immediately after sectioning. Therefore, very few artifacts will be formed by friction of the knife because of the short contact time between the very small apex of the knife and the cross section of the granules. Other artifacts (scratching, bump, etc.) due to the friction were not observed in a good section.

4.1. Observation of the inner structure of starch granules

It is very important to determine whether the resin has infiltrated starch or not when one analyzes its fine inner structure because differentiating between starch granules and infiltrating resin is difficult. Ridout et al. (2002) noted that the resin invaded starch from the results of infrared spectra of sectioned starch granules, and changed the resin so as not to infiltrate the starch granules. There are two ways for the resin to enter the granules. One is infiltration, as water travels through soil, and the other is defects, pores, and channels. Cavities of some starch granules were filled with the resin; however, those of others remained empty, as shown in Fig. 10a1 and b1. If the former is correct, starch granules not filled with the resin cannot exist. Therefore, this indicates that resin infiltration into the granule cavity occurs due to defects.

AFM observations of sectioned starch granules without cavities were performed after consideration of artifacts (Fig. 13). Fig. 13a1, a2, b1 and b2 show AFM error signal images and topographic images for the 0.3- and 0.9-μm sections, respectively. Starch granules in both sections had many wrinkles in a direction perpendicular to the knife mark and the growth rings. Although the growth rings were observed in each image, the growth rings of starch granules in the thin section were clearer than those in the thick section. The difference in clarity of the growth rings derived from the depth and width of the grooves between the growth rings occurred because starch granules in the thin section expanded wider than those in the thick section (Fig. 13a3, a4, b3 and b4). Ridout et al. (2004, 2006) proposed the swelling model in which the contrast of the growth rings is attributed to preferential swelling of the amorphous matrix of the sectioned starch granules after exposure to water. However, in our experiments, no change in corrugation of the growth rings was observed despite changing the thickness of the section. Moreover, no differences in roughness of the sectioned starch granule surface were seen between the 0.5- and 0.9-μm sections of starch granules even though the expansion

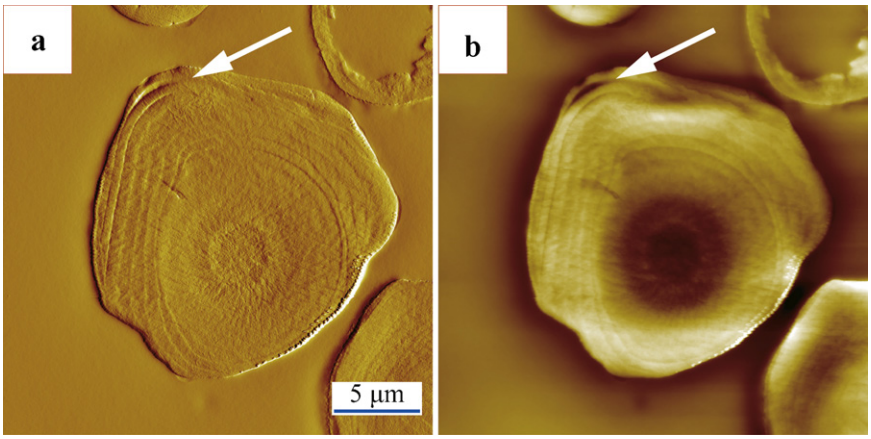

Fig. 14. AFM error signal and height images of the section of the complete granule with a crack between the growth rings indicated by white arrows.

rate was very close (data not shown). Therefore, clarification of the growth rings by water would be due to shrinkage and/or corrosion of the edge of the growth rings. In some cases, partial gelatinization and retrogradation of starch granules may have occurred due to water and low temperature drying at less than 40 °C.

Until now, two major models of starch inner structure have been proposed. One is the blocklet model (Gallant et al., 1997) in which the growth rings consist of blocklets with a diameter of 20–500 nm. The blocklet model has been supported by AFM observations (Baker et al., 2001; Neethirajan et al., 2008; Ridout et al., 2002, 2004, 2006). The other is the cluster model (French, 1972; Hizukuri, 1986) in which a side chain of amylopectin forms a double helix and becomes dense like a crystal. In the blocklet model, the blocklet consists of two or more oriented clusters of approximately 10–15 nm (Gallant et al., 1997; Putaux et al., 2000) in diameter. Gallant et al. (1997) have proposed that blocklets may comprise a single amylopectin molecule. In corn starch, the blocklet size is approximately 100 nm and 45–85 nm according to SEM (Gallant et al., 1992) and AFM results (Ridout et al., 2002), respectively. However, in our AFM images, many particles (~30 nm) were observed on the sectioned surface of starch granules (Fig. 13a5, a6, b5 and b6), and this particle size was consistent with our previous findings (Ohtani, Yoshino, Ushiki, Hagiwara, & Maekawa, 2000; Ohtani, Yoshino, Hagiwara, & Maekawa, 2000). The heights of the particles were a few nanometers less than their diameters. Probably, the difference emerges from the AFM tip radius effect and/or the degree of immersion of the particles into the growth rings. This speculation is supported by previous SAXS, XRD, and TEM studies. X-ray scattering have revealed that the crystal size of a starch granule is 9–10 nm (SAXS) (Cameron & Donald, 1992; Jenkins et al., 1993; Vermeylen, Goderis, Reynaers, & Delcour, 2004) and 14.5 nm (XRD) (Hizukuri & Nikuni, 1957), respectively. This crystal size is consistent with the cluster size observed by TEM (Gallant et al., 1997; Putaux et al., 2000). Thus, the particles observed here should be the cluster that is larger due to the AFM tip effect. The growth rings were circular near the center of the granule but formed an irregular circle in the periphery. This indicated apposition growth (Badenhuizen & Dutton, 1956; Nikuni, 1978) and that starch granules grow from the center.

Previous studies using acid and enzymatic treatment (Buttrose, 1960; French, 1984; Gallant et al., 1992; Yamaguchi, Kainuma, & French, 1979) shows that the growth ring consists of two layers; semi-crystalline and amorphous growth rings. However, we found only one layer (Fig. 13a5 and b5). Moreover, partial peeling of the growth rings due to sectioning (Fig. 14) and the SEM electron beam (observation of starch granules, data not shown) was observed. Han and Hamaker (2002) showed that starch granule proteins localize in internal concentric spheres in potato, maize, and wheat starches. It is considered that the growth rings may not be continuous but that starch synthesis may stop each ring.

5. Conclusions

Starch was embedded in resin and sectioned with a diamond knife to less than 1 μm thickness to analyze the fine inner structure of starch granules. The effects of sectioning and water in the section were studied by AFM and SEM. We obtained a clear section of starch granules by controlling the thickness of the section. As a result, our method enabled observations of distinct growth rings as observed by AFM in topographic images. The section and starch granules in the section were isotropically expanded by water as compared with the section surface and block surface. The thinner the section, the clearer the growth rings. It was considered that the contrast in the growth rings was exaggerated in the AFM images because the expansion rate of the thin section was higher than that of a thick section, and the interval of the growth rings became wider.

The granule surface was higher than the resin in our section and depressions at the center of many starch granules were observed on the section and block surfaces. Both the resin and the starch granules shrunk after the starch granules and resin were sectioned with elastic deformation. This was supported by the existence of many wrinkles, which were formed by shear stress of the knife on the sectioned surface of almost all granules perpendicular to the sectioning direction but not on starch granules of the block surface.

The presence of cavities not infiltrated by the resin indicated that the resin did not infiltrate the granules except in the presence of defects. Thus, no effect of the resin was seen in fine analysis of the corn starch granule growth rings. Thus, many particles 30 nm in size and a few nanometers in height were observed inside the growth ring layers independent of section thickness. From these results and previous small and wide angle X-ray scattering data, a particle is more likely to be a single cluster of amylopectin (~10 nm).

We found that artifacts (wrinkles, expansions, depressions) were formed on the section surface during sectioning by comparing the section surface (A and B surfaces) with the block surface using AFM and SEM. This is very important when analyzing the internal structure of starch granules on a section surface. Applying our analytical technique to other starch granules of various plant species will be useful to clarify the distribution of amylose and protein within granules. Our sectioning technique with consideration of artifacts can be applied not only to structural analyses of starch

granules but also to the analysis of the inner structure of various biological samples.

Acknowledgment

This research was supported by "Food Nanotechnology Project," MAFF, Japan.

References

Acetarin, J.-D., Carlemalm, E., Kellenberger, E., & Villiger, W. (1987). Correlation of some mechanical properties of embedding resins with their behaviour in microtomy. *Journal of Electron Microscopy Technique*, *6*, 63–79.

Akhremitchev, B. B., Broun, H. G., Graner, S. R., & Walker, G. C. (2001). Force modulation elasticity mapping of plastic-embedded, thin-sectioned skeletal muscle. *Microscopy and Microanalysis*, *7*, 32–38.

Amako, K., Takade, A., Umeda, A., & Yoshida, M. (1993). Imaging of the surface structures of epon thin sections created with a glass knife and a diamond knife by the atomic force microscope. *Journal of Electron Microscopy*, *42*, 121–123.

Badenhuizen, N. P., & Dutton, R. W. (1956). Growth of ^{14}C-labelled starch granules in potato tubers as revealed by autoradiographs. *Protoplasma*, *47*, 156–163.

Baker, A. A., Miles, M. J., & Helbert, W. (2001). Internal structure of the starch granule revealed by AFM. *Carbohydrate Research*, *330*, 249–256.

Baldwin, P. M., Adler, J., Davies, M. C., & Melia, C. D. (1998). High resolution imaging of starch granule surfaces by atomic force microscopy. *Journal of Cereal Science*, *27*, 255–265.

Black, J. T. (1971). Ultramicrotomy of embedding plastics. *Applied Polymer Symposium*, *16*, 105–125.

Blanshard, J. M. V., Bates, D. R., Muhr, A. H., Worcester, D. L., & Higgins, J. S. (1984). Small-angle neutron scattering studies of starch granule structure. *Carbohydrate Polymers*, *4*, 427–442.

Blazek, J., & Gilbert, E. P. (2010). Effect of enzymatic hydrolysis on native starch granule structure. *Biomacromolecules*, *11*, 3275–3289.

Buttrose, M. S. (1960). Submicroscopic development and structure of starch granules in cereal endosperms. *Journal of Ultrastructure Research*, *4*, 231–257.

Cameron, R. E., & Donald, A. M. (1992). A small-angle X-ray scattering study of the annealing and gelatinization of starch. *Polymer*, *33*, 2628–2635.

Chen, Y., Caib, J., Zhao, T., Wang, C., Dong, S., Luo, S., & Chen, Z. W. (2005). Atomic force microscopy imaging and 3-D reconstructions of serial thin sections of a single cell and its interior structures. *Ultramicroscopy*, *103*, 173–182.

Fannon, J. E., Hauber, R. J., & BeMiller, J. N. (1992). Surface pores of starch granules. *Cereal Chemistry*, *69*, 284–288.

French, D. (1972). Fine structure of starch and its relationship to the organization of starch granules. *Journal of the Japanese Society of Starch Science*, *19*, 8–25.

French, D. (1984). Starch: Chemistry and technology. In R. L. Whistler, J. N. BeMiller, & E. F. Paschall (Eds.), *Organization of starch granules* (2nd ed., pp. 183–247). New York: Academic Press.

Gallant, D., & Guilbot, A. (1971). Artefacts during the preparation of sections of starch granules. Studies under light and electron microscope. *Starch/Stärke*, *23*, 244–250.

Gallant, D. J., Bouchet, B., & Baldwin, P. M. (1997). Microscopy of starch: Evidence of a new level of granule organization. *Carbohydrate Polymers*, *32*, 177–191.

Gallant, D. J., Bouchet, B., Buléon, A., & Pérez, S. (1992). Physical characteristics of starch granules and susceptibility to enzymatic degradation. *European Journal of Clinical Nutrition*, *46*, S3–S16.

Gidley, M. J., & Bociek, S. M. (1985). Molecular organization in starches: A ^{13}C CP/MAS NMR study. *Journal of the American Chemical Society*, *107*, 7040–7044.

Graham, H. K., Hodson, N. W., Hoyland, J. A., Millward-Sadler, S. J., Garrod, D., Scothern, A., Griffiths, C. E. M., Watson, R. E. B., Cox, T. R., Erler, J. T., Trafford, A. W., & Sherratt, M. J. (2010). Tissue section AFM: In situ ultrastructural imaging of native biomolecules. *Matrix Biology*, *29*, 254–260.

Han, X.-Z., & Hamaker, B. R. (2002). Location of starch granule-associated proteins revealed by confocal laser scanning microscopy. *Journal of Cereal Science*, *35*, 109–116.

Hizukuri, S., & Nikuni, Z. (1957). Micelle dimension of potato starch. *Nature*, *180*, 436–437.

Hizukuri, S. (1986). Polymodal distribution of the chain lengths of amylopectins, and its significance. *Carbohydrate Research*, *147*, 342–347.

Huber, K. C., & BeMiller, J. N. (1997). Visualization of channels and cavities of corn and sorghum starch granules. *Cereal Chemistry*, *74*, 537–541.

Imberty, A., Chanzy, H., & Pérez, S. (1988). The double-helical nature of the crystalline part of A-starch. *Journal of Molecular Biology*, *201*, 365–378.

Jane, J., Kasemsuwan, T., Leas, S., Zobel, H., & Robyt, J. F. (1994). Anthology of starch granule morphology by scanning electron microscopy. *Starch/Stärke*, *46*, 121–129.

Jenkins, P. J., Cameron, R. E., & Donald, A. M. (1993). A universal feature in the structure of starch granules from different botanical sources. *Starch/Stärke*, *45*, 417–420.

Jenkins, P. J., & Donald, A. M. (1995). The influence of amylose on starch granule structure. *International Journal of Biological Macromolecules*, *17*, 315–321.

Krok, F., Szymońska, J., Tomasik, P., & Szymoński, M. (2000). Non-contact AFM investigation of influence of freezing process on the surface structure of potato starch granule. *Applied Surface Science*, *157*, 382–386.

Li, X., Ji, T., Hu, J., & Sun, J. (2008). Optimization of specimen preparation of thin cell section for AFM observation. *Ultramicroscopy*, *108*, 826–831.

Martinl, C., & Smith, A. M. (1995). Starch Biosynthesis. *Plant Cell*, *7*, 971–985.

Matsko, N. B. (2007). Atomic force microscopy applied to study macromolecular content of embedded biological material. *Ultramicroscopy*, *107*, 95–105.

Matsko, N., & Mueller, M. (2004). AFM of biological material embedded in epoxy resin. *Journal of Structural Biology*, *146*, 334–343.

Mussulman, W. C., & Wagoner, J. A. (1968). Electron microscopy of unmodified and acid-modified corn starches. *Cereal Chemistry*, *45*, 162–171.

Neethirajan, S., Thomson, D. J., Jayas, D. S., & White, N. D. G. (2008). Characterization of the surface morphology of durum wheat starch granules using atomic force microscopy. *Microscopy Research and Technique*, *71*, 125–132.

Nikuni, Z. (1978). Studies on starch granules. *Starch/Stärke*, *30*, 105–111.

Nikuni, Z., & Whistler, R. L. (1957). Unusual structures in corn starch granules. *Journal of Biochemistry*, *44*, 227–231.

Ohtani, T., Yoshino, T., Ushiki, T., Hagiwara, S., & Maekawa, T. (2000). Structure of rice starch granules in nanometre scale as revealed by atomic force microscopy. *Journal of Electron Microscopy*, *49*, 487–489.

Ohtani, T., Yoshino, T., Hagiwara, S., & Maekawa, T. (2000). High-resolution imaging of starch granule structure using atomic force microscopy. *Starch/Stärke*, *52*, 150–153.

Oostergetel, G. T., & van Bruggen, E. F. J. (1989). On the origin of a low angle spacing in starch. *Starch/Stärke*, *41*, 331–335.

Parker, M. L., Kirby, A. R., & Morris, V. J. (2008). In situ imaging of pea starch in seeds. *Food Biophysics*, *3*, 66–76.

Pérez, S., & Bertoft, E. (2010). The molecular structures of starch components and their contribution to the architecture of starch granules: A comprehensive review. *Starch/Stärke*, *62*, 389–420.

Putaux, J.-L., Buléon, A., & Chanzy, H. (2000). Network formation in dilute amylose and amylopectin studied by TEM. *Macromolecules*, *33*, 6416–6422.

Ridout, M. J., Parker, M. L., Hedley, C. L., Bogracheva, T. Y., & Morris, V. J. (2004). Atomic force microscopy of pea starch: Origins of image contrast. *Biomacromolecules*, *5*, 1519–1527.

Ridout, M. J., Parker, M. L., Hedley, C. L., Bogracheva, T. Y., & Morris, V. J. (2003). Atomic force microscopy of pea starch granules: Granule architecture of wild-type parent, r and rb single mutants, and the rrb double mutant. *Carbohydrate Research*, *338*, 2135–2147.

Ridout, M. J., Gunning, A. P., Parker, M. L., Wilson, R. H., & Morris, V. J. (2002). Using AFM to image the internal structure of starch granules. *Carbohydrate Polymers*, *50*, 123–132.

Ridout, M. J., Parker, M. L., Hedley, C. L., Bogracheva, T. Y., & Morris, V. J. (2006). Atomic force microscopy of pea starch: Granule architecture of the rug3-a, rug4-b, rug5-a and lam-c mutants. *Carbohydrate Polymers*, *65*, 64–74.

Saoudi, B., Lacapère, J.-J., Chatenay, D., Pépin, R., Derpierre, C., & Sartre, A. (1994). Imaging surface of gold-immunolabeled thin sections by atomic force microscopy. *Biology of the Cell*, *80*, 63–66.

Sterling, C. (1962). A low angle spacing in starch. *Journal of Polymer Science*, *56*, S10–S12.

Sujka, M., & Jamroz, J. (2009). α-Amylolysis of native potato and corn starches – SEM, AFM, nitrogen and iodine sorption investigations. *LWT-Food Science and Technology*, *42*, 1219–1224.

Sujka, M., & Jamroz, J. (2010). Characteristics of pores in native and hydrolyzed starch granules. *Starch/Stärke*, *62*, 229–235.

Szymońska, J., & Krok, F. (2003). Potato starch granule nanostructure studied by high resolution non-contact AFM. *International Journal of Biological Macromolecules*, *33*, 1–7.

Tang, H., Mitsunaga, T., & Kawamura, Y. (2006). Molecular arrangement in blocklets and starch granule architecture. *Carbohydrate Polymers*, *63*, 555–560.

Vermeylen, R., Goderis, B., Reynaers, H., & Delcour, J. A. (2004). Amylopectin molecular structure reflected in macromolecular organization of granular starch. *Biomacromolecules*, *5*, 1775–1786.

Whistler, R. L., Goatley, J. L., & Spencer, W. W. (1959). Effect of drying on the presence of cavities in corn starch granules. *Cereal Chemistry*, *36*, 84–90.

Yamaguchi, M., Kainuma, K., & French, D. (1979). Electron microscopic observations of waxy maize starch. *Journal of Ultrastructure Research*, *69*, 249–261.

Yamamoto, A., & Tashiro, Y. (1994). Visualization by an atomic force microscope of the surface of ultra-thin sections of rat kidney and liver cells embedded in LR white. *Journal of Histochemistry and Cytochemistry*, *42*, 1463–1470.

Zweyer, M., Troian, B., Spreafico, V., & Prato, S. (2008). SNOM on cell thin sections: Observation of Jurkat and MDAMB453 cells. *Journal of Microscopy*, *229*, 440–446.